論文 / 著書情報
Article / Book Information

Title	Simplified design procedure for controlled spine frames with energy dissipating members
Authors	Xingchen Chen, Toru Takeuchi, Ryota Matsui
Citation	Journal of Constructional Steel Research, Vol. 135, , pp. 242-252
Pub. date	2017, 8
Creative Commons	See next page.

License

Journal of Constructional Steel Research 135 (2017) 242–252

Contents lists available at ScienceDirect

Journal of Constructional Steel Research

journal homepage: www.elsevier.com/locate/jcsr

Simplified design procedure for controlled spine frames with energy-dissipating members

X. Chen*, T. Takeuchi, R. Matsui

Department of Architecture and Building Engineering, Tokyo Institute of Technology, Tokyo, Japan

ARTICLE INFO

Keywords:
Controlled spine frame system
Seismic design procedure
Simplified dual multi-degree-of-freedom model
Parametric study

ABSTRACT

A controlled spine frame system consisting of an elastic moment frame, elastic spine frame and concentrated yielding elements is proposed to ensure continuous usability of buildings in the event of an earthquake exceeding the design level. Prior studies have documented the excellent performance of spine frame structures in preventing both the concentration of damage in soft stories as well as in providing self-centering. The current study develops a simplified design method based on equivalent dual multi-degree-of-freedom and single-degree-of-freedom representations, discussing the effects of damper yield drift, and stiffness ratios between the elastic moment frame, spine frame, and dampers on the structural response. This design method is validated with a parametric study and optimal ranges of the stiffness ratios are provided.

1. Introduction

There is a high probability of large magnitude earthquakes striking major cities in Japan, particularly along the Nankai trough [1,2]. Furthermore, the buildings in these areas may be subjected to multiple events of design level intensity throughout their life. To aid rapid recovery, it is essential to ensure continued usability of buildings, particularly so for public buildings serving as post-disaster shelters or with other critical functions, such as hospitals, schools, and gymnasiums.

Previous studies have proposed and applied various spine systems in both retrofit and new build applications. Z. Qu et al. [3] employed a pivoting spine concept in the seismic retrofitting of a concrete building in Japan. B. Janhunen et al. [4] proposed a seismic retrofit solution by adding a single pivoting concrete spine to the center of a 14-story building to improve the drift pattern and distributed yielding at all levels of the building. M. Eatherton et al. [5,6] carried out a shake table test of an uplifting steel rocking frame system with post-tensioned (PT) strands to provide self-centering, and proposed several design concepts for this system. J. Lai and Mahin [7] examined the Strongback system, which combines aspects of a traditional concentric braced frame with a stiff mast to resist the tendency of damage concentration in a single or a few stories.

A controlled spine frame has been proposed by the authors, as shown in Fig. 1, and applied in the design of a new five-story research center at Tokyo Tech's Suzukakedai campus [8]. This spine frame consists of (1) a stiff braced steel frame (*i.e.*, spine frame), (2) replaceable energy-dissipating members (buckling restrained columns, BRC), and (3) envelope moment-resisting frames. The spine frame prevents the concentration of damage. Unlike the system proposed by M. Eatherton et al. [5,6], the envelope moment frames are designed to remain elastic and reduce residual drifts, providing the self-centering force without resorting to post-tensioning. The input seismic energy is absorbed by BRCs, which feature significant cumulative deformation capacity, and if required can easily be replaced following a large earthquake. This combination of structural elements reduces or effectively eliminates repair cost and downtime.

The spine frames and moment frames offer superior performance in preventing damage concentration and reducing residual deformation. However, the performance in taller structures and the effect of main structural parameters on the seismic performance are unclear. Additionally, an easy and reliable seismic design procedure is urgently required to improve the system efficiency and promote the concept in the industry. In this study, a simplified dual multi-degree-of-freedom (DMD) model was constructed to examine the dynamic characteristics of the spine frame structures. The DMD model proposed in this study is expected to exhibit nonlinear behavior similar to the full model, particularly in terms of the distribution and maximum values of story drift and shear force. Based on this model, the optimal design of the controlled spine frame structure was investigated, and a simple design procedure was proposed based on an equivalent single-degree-of-freedom (SDOF) system. A parametric study with representative design indices was conducted to compare the seismic responses of the DMD and SDOF models. Optimal ranges of key system parameters and the

* Corresponding author at: Tokyo Institute of Technology, M1-29, 2-12-1 Ookayama, Meguro-ku, Tokyo 152-8550, Japan.
E-mail address: chen.x.ad@m.titech.ac.jp (X. Chen).

http://dx.doi.org/10.1016/j.jcsr.2017.04.017
Received 22 July 2016; Received in revised form 14 April 2017; Accepted 16 April 2017

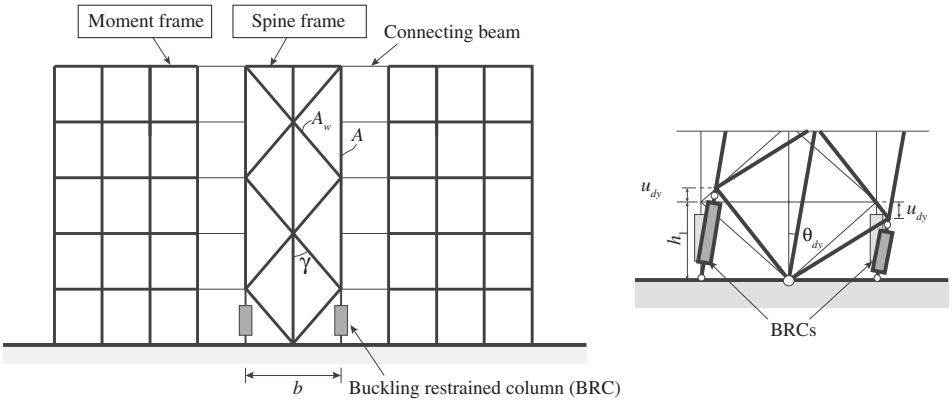

Fig. 1. The concept of a controlled spine frame structure.

applicable scope of the proposed design method was determined.

2. Analytical models for the controlled spine frames

2.1. Benchmark building structures

In order to investigate the effect of the controlled spine system, the three benchmark buildings shown in Fig. 2 were designed as per the Japanese building design codes [9], representing typical office buildings of various heights (5-story, 10-story, and 20-story). The main frames were designed to remain elastic and the damper yield strength taken as 325 MPa. As a simplifying design assumption, for this study the lateral stiffness was set proportional to the story shear, as shown in Fig. 3. However, in general, stiff spine frames provide greater latitude in story stiffness distribution, suppressing soft story formation. Simplified dual multi-degree-of-freedom models of these benchmark structures were used to validate the simplified design methods introduced in the following section.

2.2. Basic concepts and assumptions of the DMD model

A simplified dual multi-degree-of-freedom (DMD) model was constructed to clarify the key characteristics governing the response of the controlled spine frame. The concept of the DMD model used for studying the controlled spine frame is shown in Fig. 4, where the elastic moment frame and controlled spine frame are idealized as two parallel multi-degree-of-freedom (MDOF) models. The moment frame constrains the lateral deformation of the spine frame, with the connecting beams transferring only horizontal force, and it bears the weight of each story, which is represented as lumped masses.

2.3. Simplification of moment frames

The MDOF representation of the moment frame is characterized by a rotational spring representing the total flexural stiffness of the beams at a given story, and a column element representing the stiffness of all columns at a given story. The beam stiffness is conservatively calculated from centerline geometry, and the following points are neglected:

(a) Axial deformation of the beams and columns
(b) Shear deformation of the beams and columns
(c) Panel zone deformation.

This model was initially proposed by M. Nakashima et al. [10]. The original proposal assumed that the rotations of beam-column joints were identical at a given story. In contrast, in this study, it is assumed that the rotations of beam column connections at each story are inversely proportional to the corresponding beam-to-column bending stiffness ratio.

The stiffness of the rotational spring representing beams at the *i*-th story is denoted by K_{bi}, which is calculated by summing the bending moment at each beam-end M_{bij}, and dividing by the average rotation $\overline{\theta}_i$, as expressed in Eq. (1). n_{bi} is the number of beam-end at the *i*-th story.

$$K_{bi} = \sum_{j=1}^{n_{bi}} M_{bij} \Big/ \overline{\theta}_i \tag{1}$$

The columns at the *i*-th story are represented by a 4 × 4 stiffness

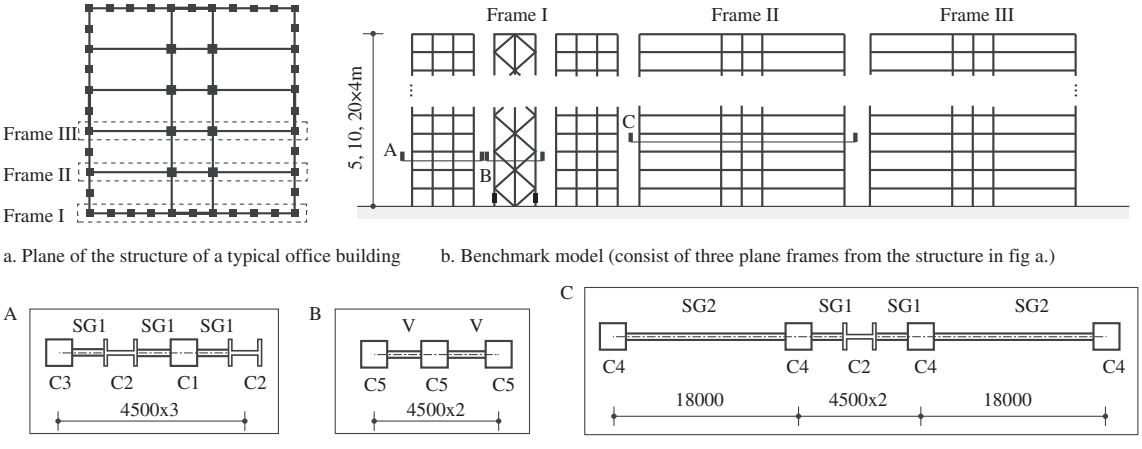

a. Plane of the structure of a typical office building b. Benchmark model (consist of three plane frames from the structure in fig a.)

c. Dimension of each frame and section of each structural member

Fig. 2. Benchmark models of the controlled spine frame structures.

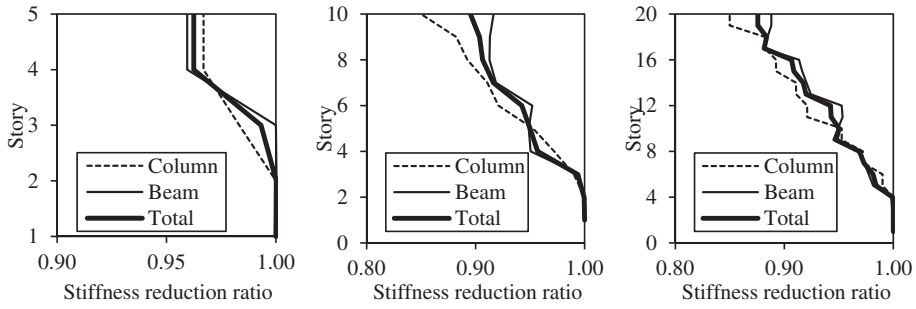

Fig. 3. Stiffness reduction ratio with respect to the height of the structures.

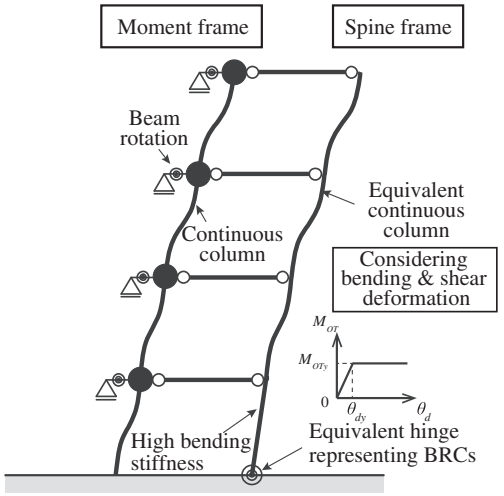

Fig. 4. Concept of the DMD model for a typical controlled spine frame structure.

matrix $[\mathbf{K_{ci}}]$, which is assembled by summing the stiffness matrices of each individual column in the original frame, and expressed by Eqs. (2) and (3):

$$\begin{Bmatrix} V_{ci}^T \\ M_{ci}^T \\ V_{ci}^B \\ M_{ci}^B \end{Bmatrix} = [\mathbf{K_{ci}}] \begin{Bmatrix} u_{i+1} \\ \theta_{i+1} \\ u_i \\ \theta_i \end{Bmatrix} \tag{2}$$

$$[\mathbf{K_{ci}}] = \begin{Bmatrix} 2\frac{K_{ci}}{h_i^2} & -\frac{K_{ci}}{h_i} & -2\frac{K_{ci}}{h_i^2} & -\frac{K_{ci}}{h_i} \\ -\frac{K_{ci}}{h_i} & \frac{2}{3}K_{ci} & \frac{K_{ci}}{h_i} & \frac{1}{3}K_{ci} \\ -2\frac{K_{ci}}{h_i^2} & \frac{K_{ci}}{h_i} & 2\frac{K_{ci}}{h_i^2} & \frac{K_{ci}}{h_i} \\ -\frac{K_{ci}}{h_i} & \frac{1}{3}K_{ci} & \frac{K_{ci}}{h_i} & \frac{2}{3}K_{ci} \end{Bmatrix}, \quad K_{ci} = 6\frac{\sum_{j=1}^{n_{ci}} EI_{cij}}{h_i} \tag{3}$$

where, I_{cij} is the second moment of area of the j-th column at the i-th story. h_i is the height of the i-th story. n_{ci} is the number of columns at the i-th story.

2.4. Simplification of spine frames

The spine frame is simplified into a single continuous column by considering both bending and shear deformation. The braces and columns are idealized as pin-connected truss elements, which only exhibit axial elongation and contraction. The equivalent stiffness in bending and shear – $(EI)_s$ and $(GA)_s$ – are expressed by Eqs. (4) and (5) [11]:

$$(EI)_s = \frac{b^2 EA}{2} \tag{4}$$

$$(GA)_s = \frac{2\cos\gamma \sin^2\gamma EA_w}{1 - \frac{A_w}{3A}\cos^3\gamma} \tag{5}$$

where, b denotes the width of the spine frame, A denotes the cross-sectional area of the columns, A_w denotes the cross-sectional area of the braces, and γ denotes the angle between the columns and braces, as shown in Fig. 1.

The stiffness of spine frames at the i-th story considering both bending and shear deformation is expressed as a 4 × 4 matrix, given by Eqs. (6) and (7):

$$\begin{Bmatrix} V_{si}^T \\ M_{si}^T \\ V_{si}^B \\ M_{si}^B \end{Bmatrix} = [\mathbf{K_{si}}] \begin{Bmatrix} u_{i+1} \\ \theta_{i+1}^s \\ u_i \\ \theta_i^s \end{Bmatrix} \tag{6}$$

$$[\mathbf{K_{si}}] = \frac{6(EI)_s}{(1+6\alpha)h_i} \begin{Bmatrix} \frac{2}{h_i^2} & -\frac{1}{h_i} & -\frac{2}{h_i^2} & -\frac{1}{h_i} \\ -\frac{1}{h_i} & \frac{2}{3}+\alpha & \frac{1}{h_i} & \frac{1}{3}-\alpha \\ -\frac{2}{h_i^2} & \frac{1}{h_i} & \frac{2}{h_i^2} & \frac{1}{h_i} \\ -\frac{1}{h_i} & \frac{1}{3}-\alpha & \frac{1}{h_i} & \frac{2}{3}+\alpha \end{Bmatrix}, \quad \alpha = \frac{2(EI)_s}{h_i^2 (GA)_s} \tag{7}$$

From the equations above we can notice that there are three global deformations at each floor of the system, namely, lateral displacement, denoted by u_i, rotation of the moment frame, denoted by θ_i, and rotation of the spine frame, denoted by θ_{is}.

Finally, the BRCs are converted into a single equivalent elasto-plastic hinge at the ground level. Bending stiffness of the column representing spine frames at the first story is assigned with a sufficient large value. The rotation of the elasto-plastic hinge is taken as $\theta_d = 2u_d / b$, as shown in Fig. 1. Therefore, the initial stiffness of the BRC hinge is expressed by $F_{dy}b^2 / 2u_{dy}$; F_{dy} and u_{dy} are the yielding axial force and deformation of each BRC.

2.5. Verification of the DMD model

The three benchmark structures introduced earlier were used to validate the DMD model. Member-by-member (MBM) models were built in OpenSees [12] and eigenvalue and time-history analysis were carried out to examine the validity of the simplified representation. The ground motions used for time history analysis included El Centro NS (1940), JMA Kobe NS (1995), TAFT EW (1925), and Hachinohe NS (1968), each 30 s long. The acceleration response spectra for the four

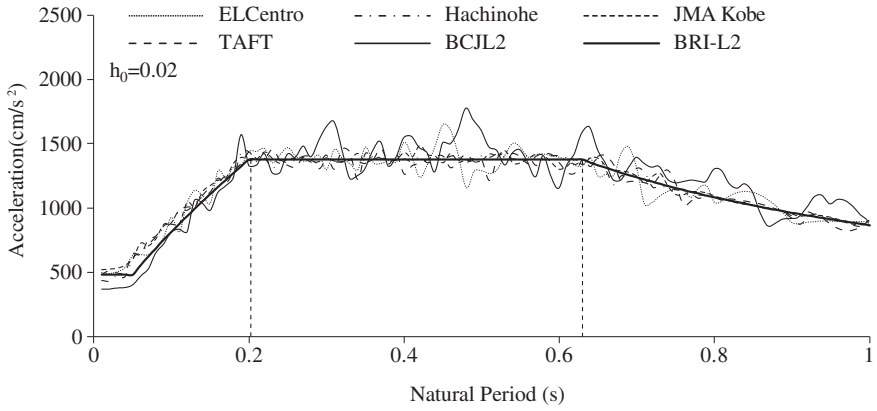

Fig. 5. Acceleration spectra of normalized input ground motions (h_0 = 0.02).

recorded ground motions were spectrally matched to follow the Japanese life-safety design spectrum (BRI-L2), as shown in Fig. 5.

Rayleigh damping was adopted for the DMD Model, with the intrinsic damping ratio h_0 set as 0.02 for the first and third modes, in order to achieve a near-constant value of damping for all modes with frequencies between these two modes.

The periods of the first three modes of DMD and MBM models are listed in Table 1. Error for the first three periods between the DMD and MBM models was < 1%, 5%, and 10% in the 5-story, 10-story, and 20-story structures, respectively. Fig. 6 compares the maximum seismic response of the three models for the DMD and MBM models. Story drift and shear force were similar in both model representations of the 5-story and 10-story structures, while the relatively large difference in the 20-story structure is primarily attributed to the axial deformation of columns in the moment frame. When the axial stiffness of the columns was considered infinite, the error in the first three periods reduced to 0.5% for each mode of each model. Therefore, the DMD model produces a good estimation of drift and shear for the 5-story and 10-story structures, but only provides the general distribution in the 20-story structure. This model representation will be used later for comparison with the SDOF model.

3. Design procedure using equivalent SDOF model

To develop a practical design method, the structure was further simplified into a single-degree-of-freedom (SDOF) model. This model neglects higher mode effects, but enables the equivalent linearization technique to be applied [13], a direct and clear method to design the system stiffness ratios and damper yield point and achieve optimal response reduction. While the benchmark buildings introduced previously featured elastic moment frames, the method introduced in this section is generalized to permit inelastic moment frames.

Table 1
Difference in the periods of the first three modes as predicted by the MBM and DMD models.

Models	Mode	MBM	DMD	Difference
5-Story	1	0.716	0.713	− 0.4%
	2	0.180	0.180	0.3%
	3	0.096	0.096	− 0.3%
10-Story	1	1.359	1.379	1.4%
	2	0.387	0.402	4.1%
	3	0.196	0.204	4.1%
20-Story	1	3.299	3.017	− 8.6%
	2	0.927	0.929	0.2%
	3	0.461	0.481	4.5%

3.1. Equivalent SDOF model of the controlled spine frame structure

3.1.1. Simplification of the main frame without BRCs

The main frame excluding the BRCs was first simplified as a MDOF model, and assembled into an equivalent SDOF model, as illustrated in Fig. 7.

The equivalent mass $M_{eq}$and height H_{eq} of the SDOF model are obtained by Eqs. (8)–(10):

$$M_{eq} = \frac{\left(\sum_{i=1}^{N} m_i \cdot \delta_i\right)^2}{\sum_{i=1}^{N} m_i \cdot \delta_i^2} \tag{8}$$

$$\delta_{eq} = \frac{\sum_{i=1}^{N} m_i \cdot \delta_i^2}{\sum_{i=1}^{N} m_i \cdot \delta_i} \tag{9}$$

$$H_{eq} = \frac{\sum_{i=1}^{N} m_i \delta_i H_i}{\sum_{i=1}^{N} m_i \delta_i} \tag{10}$$

where m_i denotes the total self-weight of the i-th floor, including the self-weight of the columns and walls in the half story above and below. δ_i denotes the elastic lateral displacement of the i-th floor against lateral forces following the first mode response distribution (Ai distribution) of the Japanese building code. H_i denotes the height from the i-th floor to the ground level.

Relation between base shear force and equivalent story drift ratio of the MDOF model obtained from pushover analysis with lateral forces following the Ai distribution was utilized as the force-deformation curve for the SDOF model. The nonlinear curve was further idealized as a bilinear curve, matching both the shear force at 2.5% drift and area under the curve up to 2.5% drift.

3.1.2. Stiffness and yielding drift of dampers

Generally, connection elements have a significant influence on the effectiveness of damping devices, reducing the imposed local deformations and achieved damping for a given level of drift. For controlled spine frame structures, the spine frame flexural stiffness reduces the effective damper stiffness and must be accounted for. To isolate the spine frame stiffness in the member-by-member model, pushover analysis is first conducted with the dampers substituted with rigid elements (Fig. 8 (a)) and secondly with the dampers removed (Fig. 8 (b)). Thus, the stiffness of the spine frame K_c can be isolated from the frame K_f by subtracting the results of the first pushover analysis (K_c + K_f) from the second K_f.

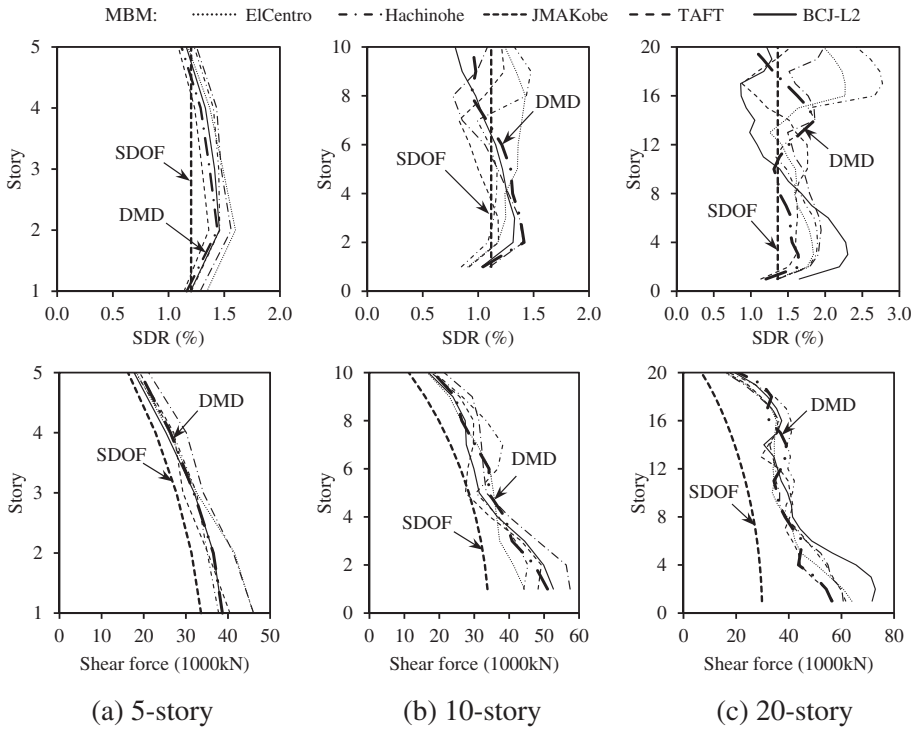

Fig. 6. A comparison of the seismic responses of MBM (5 ground motions), DMD (BCJ-L2), and SDOF (BRI-L2) models.

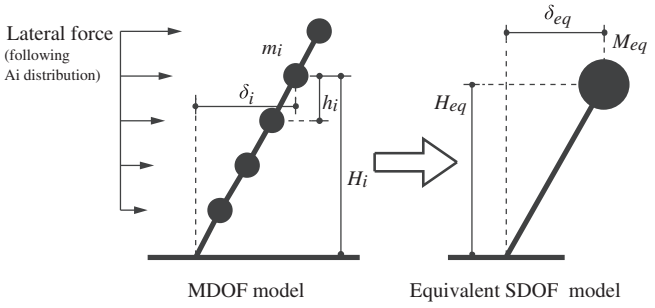

Fig. 7. Simplification of the main frame without BRCs.

Next, the local damper stiffness is calculated from Eqs. (11)–(14). The first story yield drift ratio, θ_{dy}, for now neglecting the brace shear deformation, is given by:

$$\theta_{dy} = 2u_{dy}/b \tag{11}$$

The overturning moment at the bottom of the spine frame, denoted by M_{dy}, is as follows:

$$M_{dy} = F_{dy} \cdot b \tag{12}$$

The spine frame base shear, denoted by Q_{dy}, assumes that the first-mode response is dominant and is expressed as:

$$Q_{dy} = \frac{M_{dy}}{H_{eq}} \tag{13}$$

Finally, the horizontal stiffness of the BRCs, denoted by K_d, is calculated from Eq. (14):

$$K_d = \frac{Q_{dy}}{\theta_{dy} H_{eq}} \tag{14}$$

where, u_{dy} and F_{dy} represent the axial yield deformation and force of each BRC, b represents the width of the spine frame, as shown in Fig. 9.

Fig. 8 (d) shows the full structural system, with the damper stiffness expressed by Eq. (15), including the flexural deformation of the spine frame:

$$K_a = \frac{1}{\frac{1}{K_d} + \frac{1}{K_R - K_f}} \tag{15}$$

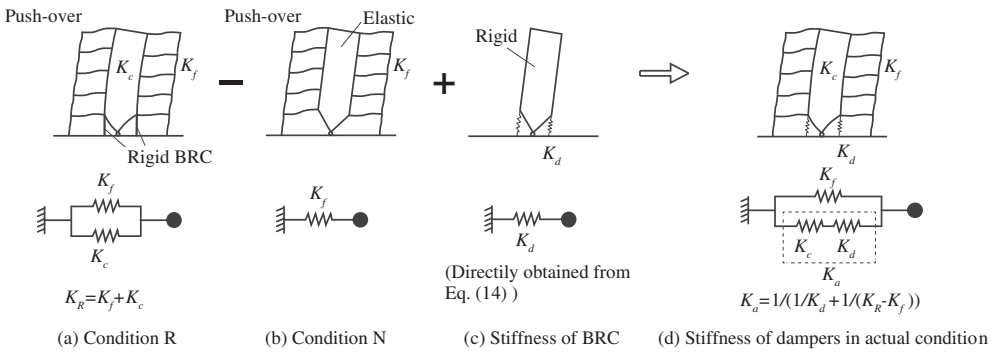

Fig. 8. Spring models for each condition.

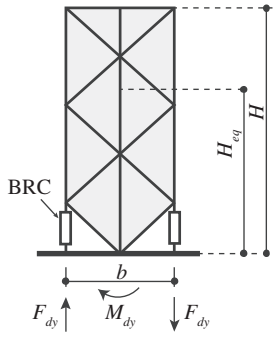

Fig. 9. An illustration of the BRCs in a spine frame.

3.2. Evaluation of equivalent damping ratio

For a given maximum story drift ratio θ_t, the equivalent damping ratio h_{eq}' can be evaluated from the strain energy and dissipated energy of the main frame and dampers, expressed by Eq. (16) and Fig. 10.

Iteration is required as damping is a function of drift, which in turn is a function of damping.

$$h_{eq}' = h_0 + \frac{E_{fp} + E_{ap}}{4\pi(E_{fe} + E_{ae})} \tag{16}$$

where, h_0 is the intrinsic viscous damping ratio; E_{fp} and E_{ap} represent the hysteretic energy of the main frame and BRCs, respectively, and E_{fe} and E_{ae} represent the equivalent elastic strain energy. The equivalent damping ratio h_{eq} of the system is calculated using Eq. (17), using an integration method originally proposed by Newmark and Rosenblueth, and described by K. Kasai et al. [14].

$$h_{eq} = h_0 + \frac{1}{\mu}\int_1^{\mu} h_{eq}'(\mu')d\mu',\quad \mu' > 1,\ h_0 = 0.02 \tag{17}$$

Equivalent damping at various yielding stages is expressed by Eqs. (18) and (19):

If $\mu_f \le 1$ and $\mu_a > 1$, then

$$h_{eq} = h_0 + \frac{2}{\pi\mu_a r}\ln\frac{(1 - r + r\mu_a)}{(\mu_a)^r} \tag{18}$$

If $\mu_f > 1$, then

$$h_{eq} = h_0 + \frac{2}{\pi\mu_a r}\ln\frac{(1 - r + r\mu_l)}{(\mu_l)^r} + \frac{1}{\mu_f}\frac{2}{\pi}\ln\frac{\left(\frac{J\mu_f + P}{J + P}\right)^{\left(\frac{P}{J} + \frac{S}{\mu_l P}\right)}}{(\mu_f)^{\frac{S}{\mu_l P}}} \tag{19}$$

where, K_{fh} denote the stiffness of the main frame after yielding, $r = \frac{K_f}{K_f + K_a}$, $\mu_f = \frac{\theta_t}{\theta_{fy}}$, $\mu_a = \frac{\theta_t}{\theta_{ay}}$, $\mu_l = \frac{\mu_a}{\mu_f}$, $P = \mu_l(1 - p) + q$, $S = (\mu_l)^2(1 - p) + q$, $J = \mu_l p$, $p = \frac{K_{fh}}{K_f}$, $q = \frac{K_a}{K_f}$.

The equivalent period T_{eq} can be evaluated from the secant stiffness K_{eq} at maximum drift θ_t, given by Eqs. (20) and (21):

If $\mu_f \le 1$ and $\mu_a > 1$, then

$$T_{eq} = T_f\sqrt{\frac{1}{1 + q/\mu_a}} \tag{20}$$

If $\mu_f > 1$, then

$$T_{eq} = T_f\sqrt{\frac{\mu_f\mu_l}{q + (1 - p + p\mu_f)\mu_l}} \tag{21}$$

where T_f is the elastic period of the main frame.

3.3. Evaluation of peak deformation and force response

The displacement response reduction factor can be expressed by Eq. (22).

$$R_d = \frac{T_{eq}}{T_f}D_h\frac{\overline{S_{pv}}(T_{eq}, h_0)}{S_{pv}(T_f, h_0)},\qquad S_{pv}(T, h_0) = \begin{cases}\frac{S_{a,\max}}{2\pi}T & (T \le T_l)\\ \frac{S_{a,\max}}{2\pi}T_l & (T > T_l)\end{cases} \tag{22}$$

The response reduction effect due to damping is given by Eq. (23)

$$D_h = \sqrt{\frac{1 + \alpha h_0}{1 + \alpha h_{eq}}} \tag{23}$$

where α is an empirical value, set as $\alpha = 25$.

The period shift effect can by simplified using the approach proposed by K. Kasai et al. [14] and is given by Eq. (24)

$$\overline{S_{pv}}(T_{eq}, h_0) = \frac{1}{T_{eq} - T_{f+a}}\int_{T_{f+a}}^{T_{eq}} S_{pv}(T, h_0)dT \tag{24}$$

The direct function for various portions of the response spectrum of the displacement reduction factor R_d is simplified to Eq. (25):

$$R_d = \begin{cases}\frac{T_{eq}}{T_f}D_h & T_l \le T_{f+a} \le T_{eq} \le T_f\\ \frac{T_{eq}}{T_f}D_h\frac{T_l(2T_{eq} - T_l) - T_{f+a}^2}{2(T_{eq} - T_{f+a})T_l} & T_{f+a} \le T_l \le T_{eq} \le T_f\\ \frac{T_{eq}}{T_f}D_h\frac{T_{eq} + T_{f+a}}{2T_l} & T_{f+a} \le T_{eq} \le T_l \le T_f\\ \frac{T_{eq}}{T_f}D_h\frac{T_{eq} + T_{f+a}}{2T_f} & T_{f+a} \le T_{eq} \le T_f \le T_l\end{cases} \tag{25}$$

where the period of the elastic components $T_{f+a} = T_f\sqrt{\frac{K_f}{K_f + K_a}}$ (≥ 0.16 s in this paper), and the constant spectral velocity region starts at $T_l = 0.864$ s. Drift ratio is then obtained from Eq. (26), with the updated ductility ratio used to recalculate h_{eq} using Eqs. (18) and

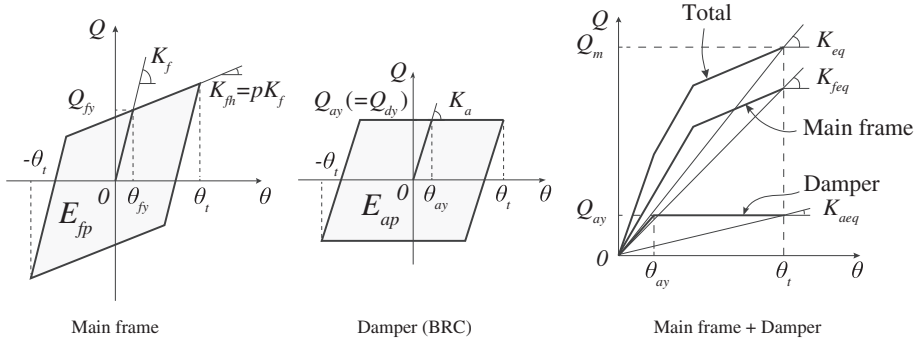

Fig. 10. Hysteretic features of the main frame and damper.

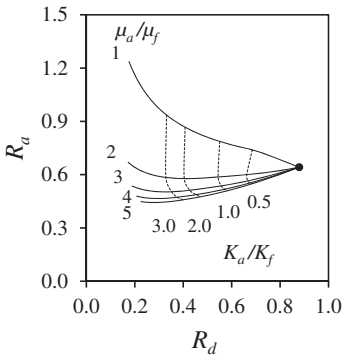

Fig. 11. Performance curve of the five-story building with a nonlinear main frame.

Table 2
Various stiffnesses of the controlled spine frame structure.

(a) Original stiffness of each component calculated from member sectional size

Story	H (mm)	$(EI)_s$ (kN·mm^2)	$(GA)_s$ (kN)	$(EI/h)_{c1}$ (kN·mm)	$(EI/l)_{b1}$ (kN·mm)
5	2×10^4	4.09×10^{14}	5.55×10^6	2.36×10^{10}	1.59×10^{10}
10	4×10^4	4.09×10^{14}	5.55×10^6	3.50×10^{10}	1.51×10^{10}
20	8×10^4	4.09×10^{14}	5.55×10^6	2.03×10^{11}	1.62×10^{10}

(b). Representative stiffness of each component for the DMD model obtained from calculations for each story level ($H_{eq}/H = 0.73$)

Story	K_{sb} (kN/mm)	K_{ss} (kN/mm)	K_s (kN/mm)	K_f (kN/mm)	K_d (kN/mm)
5	153.4	277.5	98.8	140.7	174.0
10	19.2	138.7	16.8	75.1	170.3
20	2.4	69.4	2.3	39.0	42.6

(c) Stiffness of each component obtained from a pushover analysis with lateral forces following the first-mode distribution

Story	K_f (kN/mm)	H_{eq}/H (mm)	K_d (kN/mm)	K_a (kN/mm)	K_c (kN/mm)
5	181.6	0.76	160.5	94.8	261.6
10	95.5	0.72	175.1	39.2	52.9
20	61.2	0.70	46.3	4.7	6.5

(d). Normalized stiffness obtained from the representative stiffness for the DMD model

Story	K_d / K_f	K_s / K_f	θ_{dy}
5	1.24	0.702	0.11%
10	2.27	0.224	0.11%
20	1.09	0.059	0.11%

(19), iterating until convergence is achieved.

$$\theta = R_d \theta_t^{(0)} \tag{26}$$

The resultant force is given by Eqs. (27)–(28), evaluated by equating the displacement and acceleration reduction response factors:

$$R_a = R_d \left(\frac{T_f}{T_{eq}} \right)^2 \tag{27}$$

$$Q = R_a Q^{(0)} \tag{28}$$

From Sections 3.2–3.3, the displacement reduction factor, denoted by R_d, is determined from the target story drift ratio, denoted by θ_t, the stiffness ratio of dampers and main frame, denoted by q, and the ductility factor of the dampers, denoted by μ_a, as shown in Eq. (19). Fig. 11 shows the relation between R_a and R_d for the five-story benchmark building with a nonlinear main frame. These curves are referred to as performance curves and as they are normalized, can be prepared as a generic design aid.

3.4. Simple design procedure using SDOF model

Following from the response reduction equations detailed above, a simple design procedure for the controlled spine frame using the SDOF model is proposed:

(a) Design the main frame for the target drift level without dampers (BRCs)
(b) Evaluate the elastic displacement and force response of the main frame by the response spectrum, and then calculate the displacement and force reduction factors compared to the performance targets.
(c) Select the ductility μ_a/μ_f and stiffness ratio K_a/K_f from the performance curve that satisfy the target drift ratio and acceleration response.
(d) Design the dampers for the selected ductility and stiffness, and confirm the final overall response using the equivalent linearization technique. Validate results with time-history analysis as required.

3.5. Verification of the SDOF model

The 5-, 10- and 20-story benchmark models from Section 2 were evaluated using the SDOF model, with a comparison to the DMD model shown in Fig. 6. Good agreement was achieved for the low-rise structures, but the error became notable for the 20-story structure. This is mainly due to the effect of the higher-modes response on the spine frame. The following section discusses the optimal design parameters and the applicable range of the SDOF model.

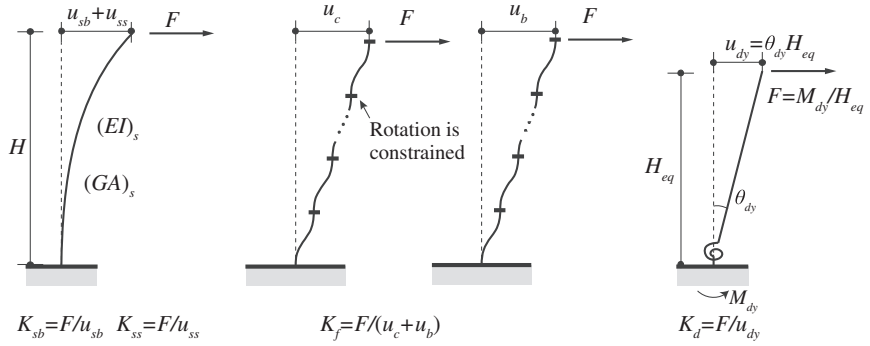

Fig. 12. Definition of representative stiffness for each component.

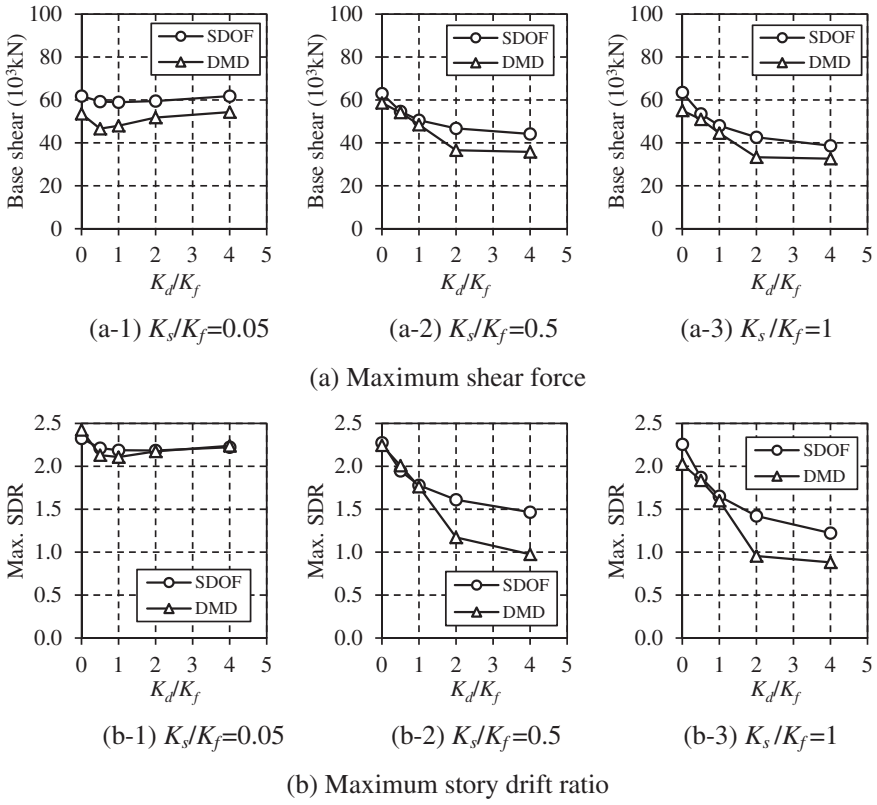

Fig. 13. Comparison of the seismic responses between the DMD and SDOF models of the 5-story structures (θ_{dy} = 0.1%).

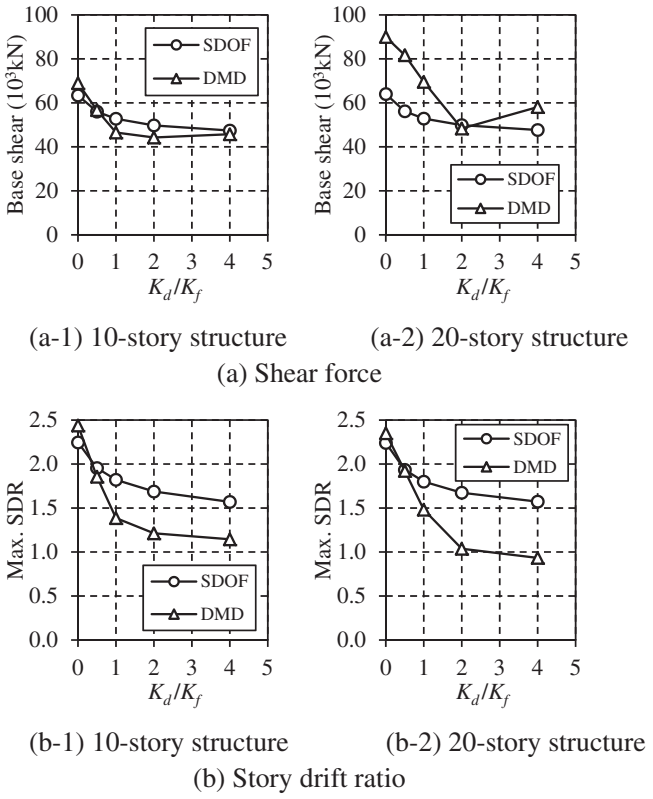

Fig. 14. Effect of the K_d/K_f ratio on the seismic responses of the 10-story and 20-story structures (K_s/K_f = 0.5, θ_{dy} = 0.1%).

4. Parametric study of controlled spine frame structures

4.1. Control parameters

A parametric study was conducted to investigate the structural characteristics of the controlled spine frame, varying the stiffness of the spine frame, moment frame, and BRCs, as well as the BRC yielding drift.

In order to simplify the parametric study, the equivalent stiffness parameter for each component is given by Eqs. (29)–(30), rather than the accurate stiffness developed for the DMD model in Section 2. The lateral stiffness of the spine frame is defined in Eq. (29) as a function of the bending stiffness K_{sb} and shear stiffness K_{ss}:

$$K_{sb} = \frac{3(EI)_s}{H^3}, \quad K_{ss} = \frac{(GA)_s}{H}, \quad K_s = \frac{1}{\frac{1}{K_{ss}} + \frac{1}{K_{sb}}} \tag{29}$$

Note that K_s is different from K_c in Fig. 8 due to different constraint conditions. It is suggested to use K_s in the primary design and K_c in the final detailed design for the spine frame.

The lateral stiffness of the moment frame is given by:

$$K_f = \frac{12}{\sum_{i=1}^{N}\left(\frac{h_i^2}{(EI/h)_{ci}} + \frac{h_i^2}{(EI/l)_{bi}}\right)} \tag{30}$$

Also note that the K_f herein slightly differs from K_f in Fig. 8 because of the simplified constraint conditions.

The lateral stiffness of BRC hinge is K_d calculated from Eq. (14) with H_{eq}/H as 0.73.

Here, H represents the structural height, $(EI/h)_{ci}$ and $(EI/l)_{bi}$ represent the sum of the line stiffness of the columns and beams at the i-th story. The stiffness of each component of the three benchmark

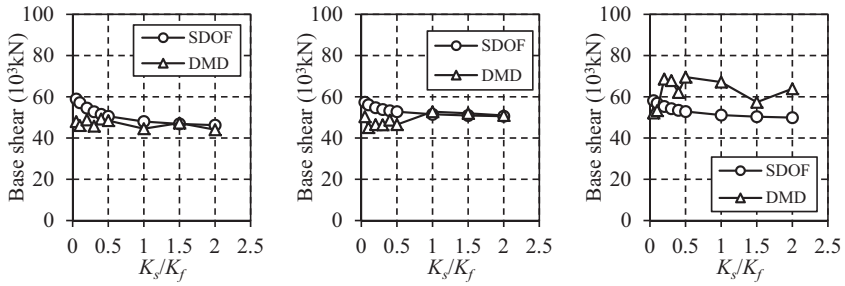

(a-1) 5-story structure (a-2) 10-story structure (a-3) 20-story structure

(a) Effect of the K_s/K_f ratio on the shear forces of the DMD and SDOF models

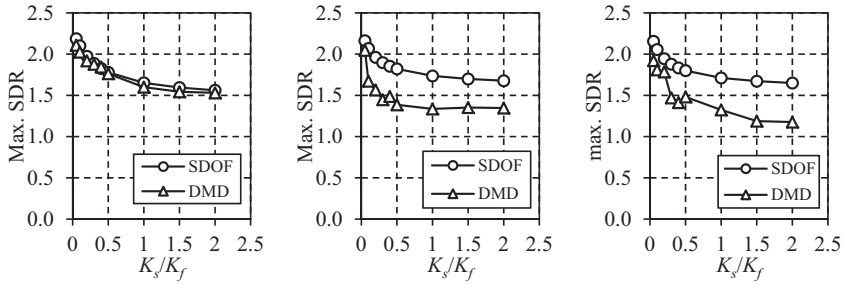

(b-1) 5-story structure (b-2) 10-story structure (b-3) 20-story structure

(b) Effect of the K_s/K_f ratio on deformation of the DMD and SDOF models

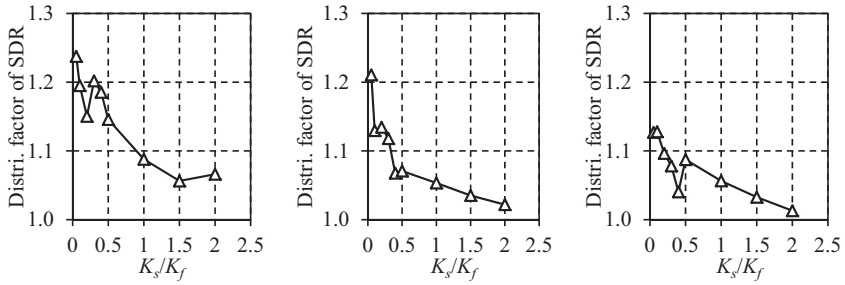

(c-1) 5-story structure (c-2) 10-story structure (c-3) 20-story structure

(c) Effect of the K_s/K_f ratio on the deformation distribution of the DMD and SDOF models

Fig. 15. Effect of the K_s/K_f ratio on the seismic responses of 5-story, 10-story, and 20-story structures (K_d/K_f = 1, θ_{dy} = 0.1%).

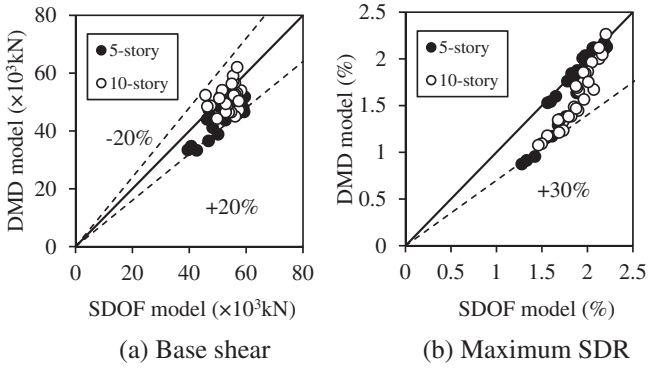

(a) Base shear (b) Maximum SDR

Fig. 16. Validation of the proposed design procedure via SDOF models ($0.5 \le K_d/K_f \le 2.0$, $0.05 \le K_s/K_f \le 2.0$, for 5-story and 10-story structures).

structures is listed in Table 2, referring to Fig. 12.

The response of a controlled spine frame can be characterized by the normalized damper-to-moment frame stiffness ratio, denoted by K_d/K_f, and spine-to-moment frame stiffness ratio, denoted by K_s/K_f. These are summarized in Table 2 (d). The range investigated in this study was selected to represent realistic code-compliant and buildable structures. Namely, K_d/K_f ranged from 0.5 to 8.0, and K_s/K_f ranged from 0.05 to 2.0. The specific values selected for the 5-story structure are listed in Table 3 as an example.

4.2. Optimal design using design indices

The parametric study was used to validate the proposed simplified SDOF model against the DMD model, examine the response trends and influence of the various control parameters, and finally to optimize the stiffness ratios K_d/K_f and K_s/K_f. Applying the seismic input shown in Fig. 5, the peak story drift ratio and shear force as a function of K_d/K_f are shown in Figs. 13 and 14. Generally, the simplified SDOF method slightly overestimates the base shear and maximum story drift ratios.

As illustrated in Fig. 13 for the 5-story structure, increasing K_d/K_f results in decreasing deformations and shear forces for the simplified SDOF method. Generally, the base shear of the DMD and SDOF models are in good agreement when $K_d/K_f \le 1.0$. For exceptionally large dampers with K_d/K_f in the range of 2.0–4.0, a significant discrepancy was observed with respect to the deformations between SDOF and DMD

Table 3
Value of each parameter for various cases of the 5-story structure (θ_{dy} = 0.1%).

Case	K_f (kN/mm)	K_d (kN/mm)	K_d/K_f	A_c (mm^2)	L_p (mm)
5Kdf0.5θy1		70.4	0.5	5129	
5Kdf1θy1	140.7	140.7	1	10258	3650
S5Kdf2θy1		281.4	2	20518	
5Kdf4θy1		562.8	4	41032	

Case	K_s (kN/mm)	K_s/K_f
S5Kdf1Ksf0.05θy1	7.04	0.05
S5Kdf1Ksf0.1θy1	14.1	0.1
S5Kdf1Ksf0.2θy1	28.1	0.2
S5Kdf1Ksf0.3θy1	42.2	0.3
S5Kdf1Ksf0.4θy1	56.3	0.4
S5Kdf1Ksf0.5θy1	70.4	0.5
S5Kdf1Ksf1.0θy1	140.7	1.0
S5Kdf1Ksf1.5θy1	211.1	1.5
S5Kdf1Ksf2.0θy1	281.4	2.0

methods. This is mainly because the SDOF models assume a post-yield response distribution, thus the SDOF model provides better estimation for structures developing into sufficient plasticity, or structures in which the response distribution doesn't change much after the yielding mechanism occurs. Therefore, it is recommended that K_d/K_f should be < 2.0 when the SDOF method is applied. Additionally, at least a reasonable damper stiffness of $K_d/K_f \geq 0.05$ should be provided to effectively control the seismic response.

A similar trend for K_d/K_f could be observed in the results of the 10-story and 20-story structures, as shown in Fig. 14. In Fig. 14 (b-1) and (b-2), the story drift ratios of the DMD and SDOF models generally agree when K_d/K_f is < 1.0. The shear force of the DMD model exceeded that of the SDOF model in the 20-story structure, except for the case when K_d/K_f = 2.0. This indicates that the SDOF model is not suitable for tall buildings with significant higher-mode effects.

Fig. 15 demonstrates the effect of the spine-to-moment frame stiffness ratio K_s/K_f on the seismic response of the 5-story, 10-story, and 20-story structures, with the other parameters held constant at K_d/K_f = 1, and θ_{dy} = 0.1%. As observed in Fig. 15 (a), base shear is relatively independent of K_s/K_f. However, the shear force obtained by using the DMD model in Fig. 15 (a-3) exhibited significant fluctuations in the 20-story structures. These fluctuations in the higher structures are attributed to the higher-mode effect. As shown in Fig. 15 (c), concentration of SDR (that is, the maximum SDR divided by the average SDR among all the stories) decreased rapidly when K_s/K_f increased from 0 to 0.5 in all the three structures, and continued to rapidly decrease when K_s/K_f increased to 1.5 in the 5-story structure. Thus, higher K_s/K_f is strongly associated with a more uniform SDR distribution.

For the full range of K_s/K_f, the proposed simplified evaluation method is able to predict the seismic performance within an acceptable margin for both the deformation and force response of the 5-story and 10-story structures, and deformation response of the 20-story structure. However, increasing K_s/K_f cannot eliminate the higher-mode effect on shear forces, and so the simplified procedure cannot accurately predict the force response of the 20-story structure.

Fig. 16 compares the peak shear force and story drift ratio of the DMD models with those of the SDOF models for K_d/K_f of 0.5–2.0 and K_s/K_f of 0.05–2.0 in 5-story and 10-story structures. Generally, the proposed design procedure slightly overestimates the base shear and maximum story drift ratios, with the one exception being that base shear of the taller 10-story structures was underestimated. General trends are captured, and error is controlled to within approximately 20% for the base shear and 30% for the maximum story drift ratios.

Equivalent mass and shear force for each mode were calculated in order to examine the minimum first mode participation factor required for the single first mode response to be considerate sufficiently representative of the overall response. With respect to the 5-story structure, the first modal contribution factor for shear force was always higher than 83% and the response in all the cases was dominated by the first-mode. With respect to the 10-story and 20-story structures, the first modal contribution factor for shear force could only reach 76% and 59% even when K_s/K_f = 12.0, which is unrealistic large in actual application. This indicates that the accuracy of the SDOF method gradually decreases as the structure height increases due to the effects of the higher modes.

5. Conclusions

In this study, a seismic design and evaluation method has been proposed for the structural system with controlled spine frames. A parametric study was conducted to examine suitable values for key structural parameters. The following conclusions were drawn from this study:

(1) A graphical performance curve has been proposed to efficiently select the damper yield drift and damper-to-frame stiffness ratio K_d/K_f. This is a practical method to quickly arrive at optimal designs that achieve the force and deformation performance targets. The optimal stiffness K_d/K_f ratio typically falls between 0.5 and 2.0.
(2) The stiff spine frame has a dramatic effective in achieving a more uniform deformation distribution along the height of a structure. To ensure the effectiveness of the dampers, K_s/K_f should exceed 0.5.
(3) Increasingly stiff dampers lead to a more significant difference between the SDOF models and the DMD models. It is recommended that the spine-to-moment frame stiffness ratio K_d/K_f should not exceed 2.0 for the typical case of $0.5 \leq K_s/K_f \leq 2.0$ for using the SDOF models.
(4) The proposed simplified design procedure based on the SDOF model is valid for structures in which the first modal contribution factor for shear force exceeds 80%. This corresponds to ordinary spine frame structures not taller than 10 stories and spine-to-moment frame stiffness ratios K_s/K_f of 0.5 to 2.0.

Abbreviations

DMD simplified dual MDOF model for controlled spine frame structures
SDR story drift ratio

Acknowledgement

This research was supported by JSPS KAKENHI Grant number 16J04449.

References

[1] "Final report on damage and countermeasure of major earthquakes predicted to occur near capital of Japan." Cabinet Office of Government of Japan. 2013.12 (in

Japanese).
[2] “Final report on countermeasure of major earthquakes predicted to occur along Nankai trough.” Cabinet Office of Government of Japan. 2013.5 (in Japanese).
[3] Z. Qu, A. Wada, S. Motoyui, H. Sakata, S. Kishiki, Pin-supported walls for enhancing the seismic performance of building structures, Earthq. Eng. Struct. Dyn. 41 (2012) 2075–2091, http://dx.doi.org/10.1002/eqe.2175.
[4] B. Janhunen, S. Tipping, J. Wolfe, Seismic retrofit of a 1960s steel moment-frame high-rise using a pivoting spine, Annual Convention of the Structural Engineers Association of California, 2013, pp. 320–336.
[5] M. Eatherton, J. Hajjar, X. Ma, H. Krawinkler, G. Deierlein. Seismic design and behavior of steel frames with controlled rocking—part I: concepts and quasi-static subassembly testing. The 2010 NASCC & Structures Congress, Orlando, USA: 1523–1533. http://dx.doi.org/10.1061/41130(369)138.
[6] M. Eatherton, X. Ma, H. Krawinkler, D. Mar, S. Billington, J. Hajjar, G. Deierlein, Design concepts for controlled rocking of self-centering steel-braced frames, J. Struct. Eng. 140 (11) (2014), http://dx.doi.org/10.1061/(ASCE)ST.1943-541X.0001047 (04014082).
[7] J. Lai, S. Mahin, Strongback system: a way to reduce damage concentration in steel-braced frames, J. Struct. Eng. 141 (9) (2014), http://dx.doi.org/10.1061/(ASCE)ST.1943-541X.0001198 (04014223).
[8] T. Takeuchi, X. Chen, R. Matsui, Seismic performance of controlled spine frames with energy-dissipating members, J. Constr. Steel Res. 114 (2015) 51–65, http://dx.doi.org/10.1016/j.jcsr.2015.07.002.
[9] The building standard law of Japan. The Building Center of Japan. 2013.11.
[10] M. Nakashima, K. Ogawa, K. Inoue, Generic frame model for simulation of earthquake responses of steel moment frames, Earthq. Eng. Struct. Dyn. 31 (2002) 671–692.
[11] T. Saka, Load Bearing Capability Analysis of Double-layer Truss Plates With Continuous Shell Analogy, (1988), p. 12 (PhD Thesis, in Japanese).
[12] Open system for earthquake engineering simulation (OpenSees) version 2.5.0. Sponsored by Pacific Earthquake Engineering Research Center (PEER), University of California, Berkeley, Available from: http://opensees.berkeley.edu (last accessed May 2016).
[13] M. Kobayashi, N. Hayashi, Y. Izawa, T. Koh, Damage control of passively vibration-controlled mid and high rise buildings considering plasticity behavior of frames, J. Struct. Construction Eng. 592 (2005) 59–66 (in Japanese, Architecture Institute of Japan).
[14] K. Kasai, H. Ito, A. Watanabe, Peak response prediction rule for a SDOF elasto-plastic system based on equivalent linearization technique, J. Struct. Construction Eng. 571 (2003) 53–62 (in Japanese, Architecture Institute of Japan).